Mass transfer in channels in the presence of wall transpiration

M. Ciofalo*, M. Di Liberto, L. Gurreri, M. La Cerva, L. Scelsi
Dipartimento dell'Innovazione Industriale e Digitale, Università di Palermo, Italy
*Corresponding author; email michele.ciofalo@unipa.it

Abstract. Mass transfer to or from transpiring walls is studied. Examples from different fields of engineering, notably involving membrane processes, are illustrated, and analogies or differences with respect to heat transfer problems are discussed. With special reference to plane channel flow, suitable dimensionless parameters are introduced, and the dependence of the Sherwood number upon these parameters is computed by a number of approaches of different complexity, from two-dimensional CFD to simple algebraic correlations.

1. General aspects of wall transpiration

A *transpiring* wall is a surface, adjacent to a boundary layer or channel flow, through which fluid is made to pass either into the main stream (*injection*, or *blowing*) or out of it (*suction*). It is generally understood that the transpiration areal flow rate is much less than the main flow rate and that the direction of the transpiring flow is orthogonal to the wall.

In the case of suction, the transpiring fluid is necessarily the same as the main one. In injection, or blowing, it may be the same or different. Transpiration may occur either through a porous (permeable) wall or through physically distinct orifices in an otherwise impermeable wall, see Figure 1.

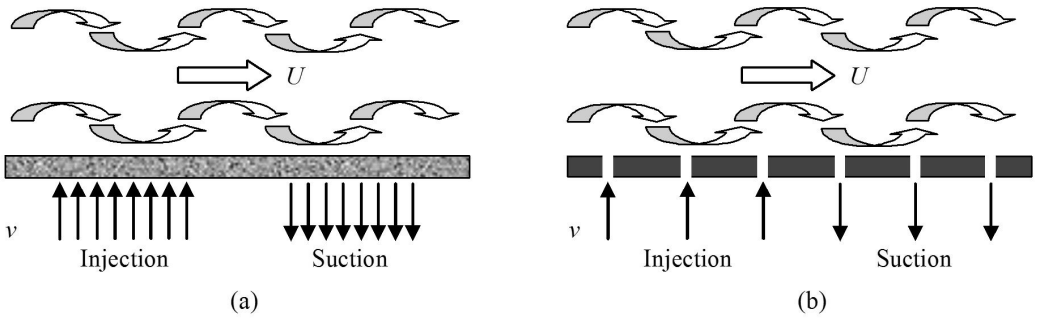

Figure 1. Transpiring walls with either injection (blowing) or suction: (a) porous; (b) perforated.

Transpiration modifies velocity profiles and, if any, temperature or other scalar profiles in the main flow, and thus affects momentum, heat and mass transfer between the main fluid stream and the wall. Therefore, it has been studied for a long time, either experimentally or by analytical / numerical techniques, in connection with such problems as:

- Boundary layer control [1, 2].
- Transpiration cooling, i.e. protecting solid surfaces (e.g. turbine blades [3] or re-entry vehicles [4]) from a high-temperature gas flow by blowing.

- Prevention of scaling in processes like supercritical water oxidation [5].

Moreover, it should be observed that phenomena of evaporation / condensation from / to a wall-adjacent liquid film (Figure 2), as may occur, for example, in nuclear reactor containment cooling problems [6], exhibit strong analogies with transpiration (blowing / suction) phenomena, so that their prediction can benefit from the modelling efforts devoted to these latter.

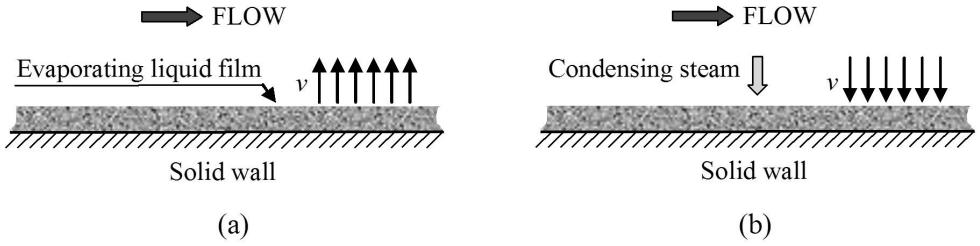

Figure 2. Evaporating (a) or condensing (b) liquid films, approaching blowing / suction conditions.

From these studies, the following synthetic conclusions can be drawn:

a) In laminar boundary layers, suction delays transition to turbulence [2].
b) Both in laminar and turbulent boundary layers, blowing reduces friction and heat transfer from the fluid stream to the wall, while suction increases them [1, 7]. For example, Figure 3 (adapted from reference [1]) reports the Stanton number St_x (based on the distance x from the leading edge) in a flat plate boundary layer as a function of the blowing factor v/U_∞ (positive for injection, negative for suction) for three values of the x-based Reynolds number Re_x. It can be observed that St_x tends to zero for $v/U_\infty \to \infty$ (large injection), while it tends to $-v/U_\infty$ (and thus diverges) for $v/U_\infty \to -\infty$ (large suction). The Reynolds number has but a minor influence on this behaviour.
c) In transpired boundary layers, a similar behaviour is exhibited by the Stanton number and the friction coefficient, so that the Reynolds analogy ($St_x = C_f/2$) continues to hold (at least approximately).

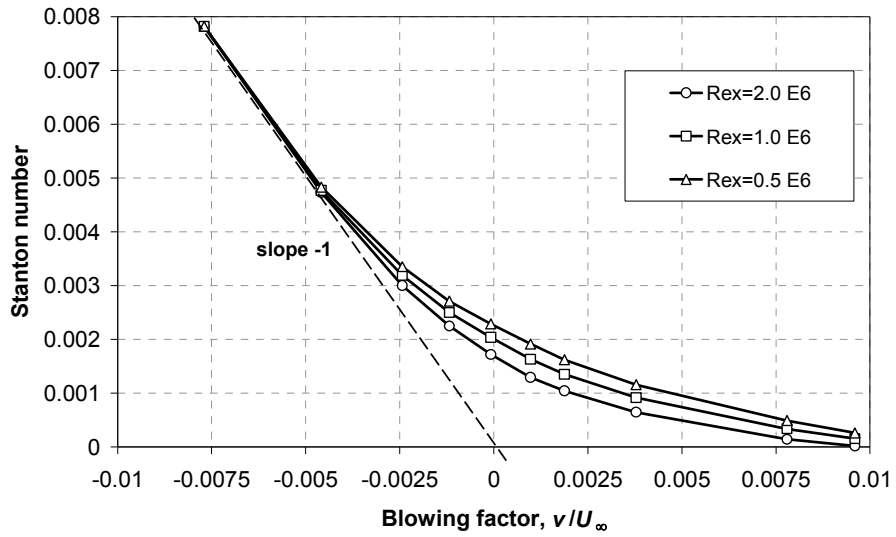

Figure 3. x-Stanton number as a function of the blowing factor for three different values of the x-Reynolds number (adapted from Kays and Moffat 1975).

2. Mass transfer with transpiring walls

2.1 Preliminary remarks on mass vs. heat transfer

Most of the problems studied in the literature in connection with transpiring walls regard phenomena of heat or momentum transfer. The present work focuses on the influence of wall transpiration on *mass* transfer. In order to avoid misunderstandings, a few preliminary remarks are appropriate:

a) Wall transpiration, of course, is in itself a process of mass transfer between a wall and a fluid stream, since the transpiration flow carries its own mass. However, by "mass transfer" we denote here a separate process involving the transfer of a massive species other than the carrying fluid, i.e. a component dispersed in the fluid either at molecular/ionic scale (e.g. salt) or at a coarser scale (e.g. small solid particles). For the sake of simplicity, in all these cases we will call the carrier fluid the "solvent" and the dispersed component the "solute". As better specified in the examples that follow, such processes occur in electrodialysis, reverse osmosis, filtration and usually involve the use of membranes.

b) As it is well known, a close analogy exists between heat and mass transfer. However, mass transfer phenomena present some peculiar characteristics of their own. First, the transfer of a solute, unlike that of heat, affects the mass balance of the solution. Second, a solute is usually characterized by Schmidt numbers (10^2-10^3) much higher than the Prandtl number of common fluids (except, of course, highly viscous fluids). Finally, selective barriers exist that can prevent the passage of the solute along with the solvent through a wall (which is about impossible with heat).

2.2 Diffusive and convective mass fluxes

The total wall to bulk mass flux j_S (in kg m^{-2} s^{-1}) can always be expressed as the sum of a diffusive component $j_{diff} = -\rho D(\partial C/\partial y)_w$ and a convective component $j_{conv} = \rho v C_w$:

$$j_S = j_{diff} + j_{conv} = -\rho D(\partial C/\partial y)_w + \rho v C_w \tag{1}$$

in which D is the solute diffusivity (in m^2 s^{-1}), C is the "solute" concentration (expressed as a mass fraction, e.g. in kg/kg), the suffix w denotes the transpiring wall, and y is the direction normal to it.

Figure 4 compares concentration profiles and mass fluxes for channels with transpiring and non-transpiring walls at a given bulk concentration C_b and a given wall mass flux j_S directed into the fluid (i.e., positive). Graph (a) refers to the reference case of no traspiration. In this case, the mass flux at the wall is purely diffusive. Graph (b) is for a channel with positive transpiration (injection, or blowing). Here C_w, C_w-C_b and the diffusive mass flux $-\rho D(\partial C/\partial y)_w$ decrease with respect to the non-traspiring case (a), but this reduction is compensated by a positive (into the fluid) convective heat flux $\rho v C_w$, so that the overall mass transfer coefficient k increases. On the contrary, graph (c) is for a channel with negative transpiration (suction) of the same intensity as in case (b). Here C_w, C_w-C_b and the diffusive mass flux $-\rho D(\partial C/\partial y)_w$ increase with respect to the non-traspiring case (a), but this increment is compensated by a negative (out of the fluid) convective heat flux $-\rho v C_w$, so that the overall mass transfer coefficient k decreases.

The total mass transfer coefficient k (m s^{-1}) can be defined as the ratio of the total solute mass flux j_S into the channel and the difference between wall and bulk volumetric concentrations ρC_w, ρC_b (in which ρ is the solution density in kg m^{-3}). The coefficient k can then be made dimensionless as a Sherwood number:

$$\mathrm{Sh} = \frac{j_S}{(C_w - C_b)} \cdot \frac{d_{eq}}{\rho D} \tag{2}$$

in which d_{eq}=2H is a suitable length scale, e.g. the hydraulic diameter of the channel.

Also diffusive and convective Sherwood numbers can be separately defined as

$$\mathrm{Sh}_{diff} = \frac{j_{diff}}{(C_w - C_b)} \cdot \frac{d_{eq}}{\rho D} = -\frac{d_{eq}}{(C_w - C_b)} \left(\frac{\partial C}{\partial y} \right)_w \tag{3}$$

$$\mathrm{Sh}_{conv} = \frac{j_{conv}}{(C_w - C_b)} \cdot \frac{d_{eq}}{\rho D} = \frac{C_w}{(C_w - C_b)} \cdot \frac{v d_{eq}}{D} \tag{4}$$

in which the group $v \cdot d_{eq}/D$ in Eq. (4) can be regarded as a transpiration Péclet number, Pe_{tr}. Of course, one has $\mathrm{Sh}=\mathrm{Sh}_{diff}+\mathrm{Sh}_{conv}$.

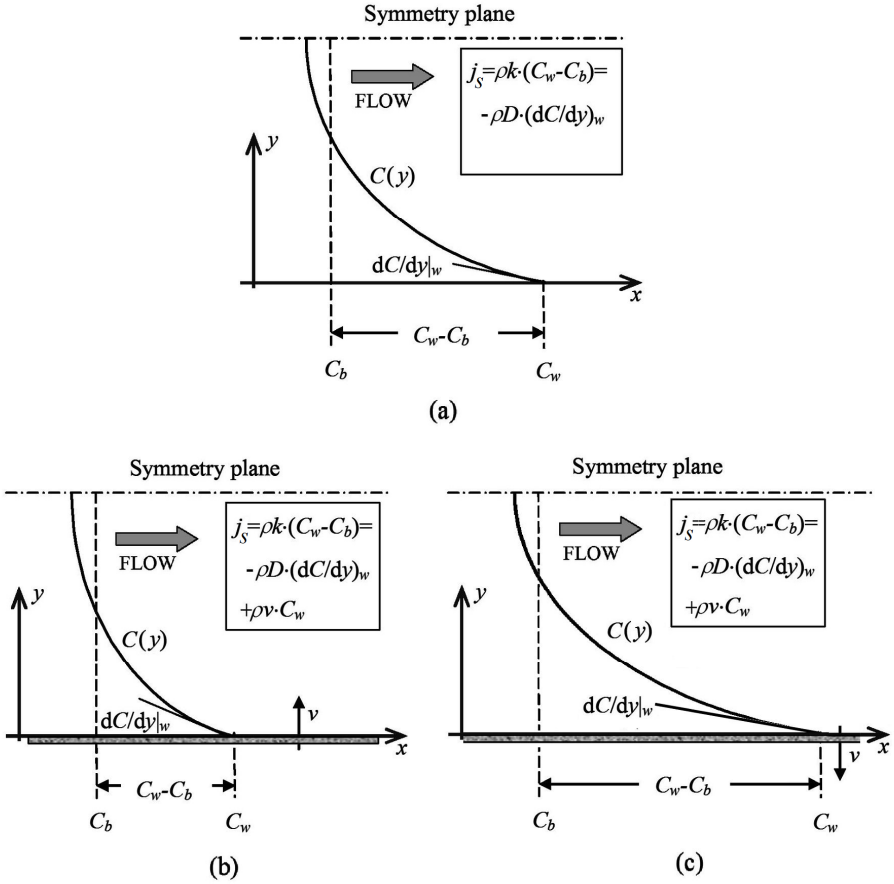

Figure 4. Concentration profiles and mass fluxes for transpiring and non-transpiring walls at the same bulk concentration C_b and mass flux j_S. (a) No transpiration. (b) Positive transpiration (blowing). (c) Negative transpiration (suction).

2.3 Examples of mass transfer processes involving wall transpiration

Processes exhibiting the whole possible set of sign combinations for the fluxes of solute (salt) and solvent (water) into or from the channels are electromembrane processes, and in particular Reverse Electrodialysis (RED) and Electrodialysis (ED) [8, 9]. This is illustrated in Figure 5.

In Reverse Electrodialysis, Figure 5(a), electrical energy is harvested from the salinity gradient between two solutions. The figure shows a repetitive unit of a real RED device (stack), comprising a concentrate channel (*CONC*), a diluate channel (*DIL*), an Anion Exchange Membrane (AEM) and a Cation Exchange Membrane (CEM). With ideal membranes, only anions and cations (e.g., Cl- and Na+) would flow from *CONC* to *DIL*. However, real membranes exhibit a finite osmotic permeability, so that water flows from the dilute to the concentrate solution. Therefore, in the concentrate channels

salt (in ionic form) flows out of the solution while water enters it (injection); on the contrary, in the diluate channels salt flows into the solution while water exits it (suction).

In Electrodialysis, Figure 5(b), electrical energy is used to create or enhance a salinity gradient between two solutions. The figure shows a repetitive unit, physically identical to a RED one. In the presence of osmotic fluxes, in the concentrate channels both salt and water flow into the solution (injection), while, in the diluate channels, both salt and water flow out of the solution (suction).

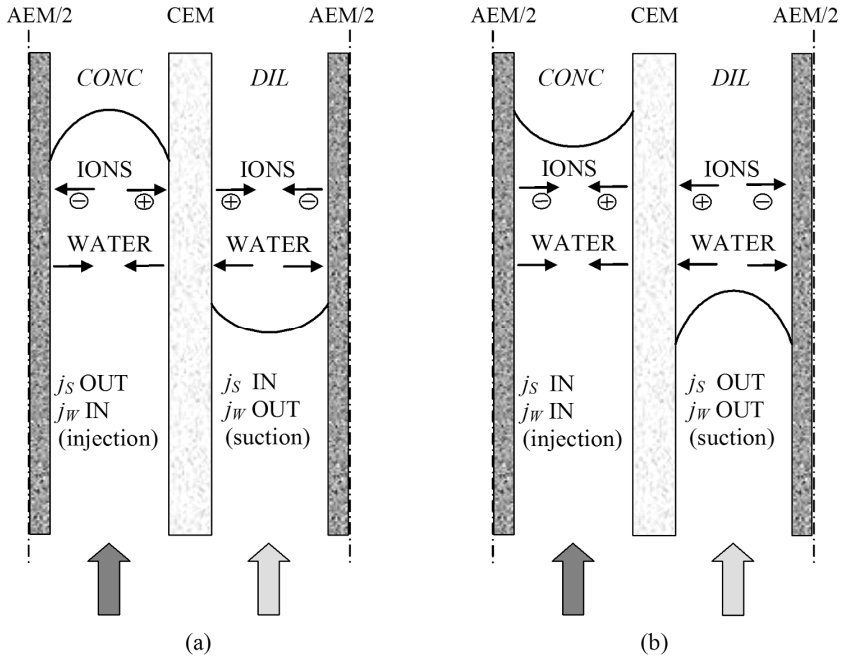

Figure 5. Concentrations and fluxes in cell pairs for reverse electrodialysis (a) or electrodialysis (b), exhibiting all possible sign combinations of solute (salt) and water fluxes.

There are also situations in which, despite the net solute mass flux being nil, solving a mass transfer problem is crucial for design and performance prediction [10]. Figure 6 shows the main mass transfer phenomena occurring in cross-flow filtration and reverse osmosis (RO). Here the wall is a selective membrane and the driving force is a trans-membrane pressure, pushing the continuous phase (solvent) out of the duct while the passage of the dispersed phase (solute) is prevented. The solute concentration builds up near the wall, causing a wall-to-fluid diffusive flux of solute $j_{diff}=-\rho D(\partial C/\partial y)$. At the same time, the y-component v of the solvent velocity causes a fluid-to-wall convective flux $j_{conv}=-\rho vC$. At the wall (y=0), the two fluxes compensate each other (for a perfectly selective membrane), i.e.

$$j_S = -\rho D(\partial C/\partial y)_w - \rho v C_w = 0 \tag{5}$$

which is just a form of Eq. (1).

The main problem is usually that of determining the trans-membrane pressure Δp to be applied to provide a given flux v of solvent (or *vice versa*). The problem would be trivial if Δp depended only on v, but is made more complex by the fact that it also depends on the near-wall concentration C_w. Eq. (5) can be regarded as a third type (Robin) wall boundary condition for the concentration C, allowing – once v is imposed – the solution of a solute transport equation and thus the assessment of C_w [11]. If the diffusive mass transfer coefficient k_{diff} (i.e., the diffusive Sherwood number Sh_{diff}) is known, the solution of the C-transport equation is not required since one has $-D(\partial C/\partial y)_w = k_{diff}(C_w - C_b)$, which, together with Eq. (5), gives $C_w = k_{diff} C_b /(k_{diff} + v)$.

Once v is imposed and the consequent near-wall solute concentration C_w is known, an independent equation linking the trans-membrane pressure with v and C_w is now required. In RO, it can be formulated by the Spiegler-Kedem model [11]:

$$v = K\,[\Delta p - \sigma \Delta \pi(C_w)] \tag{6}$$

in which K is a permeability coefficient, σ is the rejection coefficient (close to 1) and Δp, $\Delta \pi$ are the static and osmotic trans-membrane pressure differences, the latter being a function of near-wall concentration. Together, Eqs. (5) and (6) (in conjunction with either the solution of a transport equation for C or the knowledge of Sh_{diff}) allow the prediction of the value of Δp necessary to sustain a water flux v, or *vice versa*.

In *filtration* problems (including microfiltration, ultrafiltration, nanofiltration) Eq. (6) is replaced by equivalent relations linking the trans-membrane Δp to the water flux and to the near-wall concentration, usually by expressing the permeability coefficient K as a function of C_w.

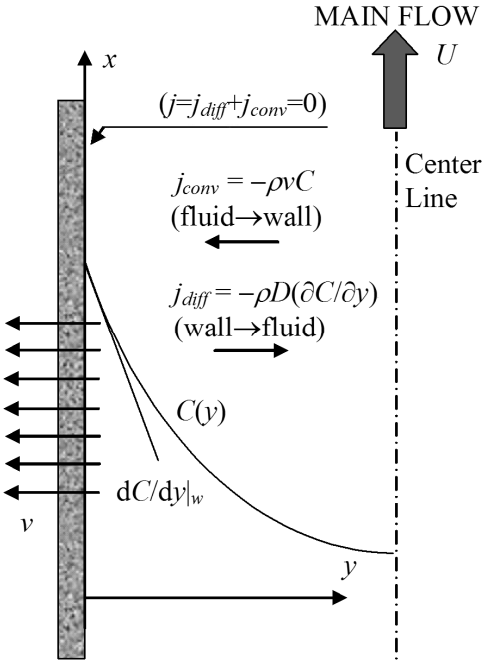

Figure 6. Mass transfer in cross-flow filtration and reverse osmosis, with zero net solute flux.

3. Models and results

3.1 Computational domain and basic assumptions

The test geometry considered in this study is the two-dimensional channel schematically shown in Figure 7. It is characterized by length L in the x-direction and thickness H in the y-direction; the origin is placed on a wall at the inlet, and symmetry about the centreline is assumed, so that the computational domain includes only half channel ($0 \le y \le H/2$). The working fluid (solution) enters with uniform velocity U_i and concentration C_i (solute mass fraction). Both the solute (with mass flux j_S) and the solvent (with cross-stream velocity v, i.e. mass flux ρv) can cross the transpiring wall; j_S and v are taken to be positive for inflow, negative for outflow. Two generic profiles of velocity and concentration are shown.

Although the problem's treatment and the results are quite more general, this configuration can be regarded as representative of a generic, flat solution channel belonging to a stack for electrodialysis, reverse electrodialysis or similar membrane processes, as shown in Figure 5. In most cases, the solvent

was assumed to be water and the solute an electrolyte such as NaCl or NaOH. The channel thickness H was fixed to 300 μm ($3 \cdot 10^{-4}$ m) and the length L to 0.6 m, so that L/d_{eq}=1000.

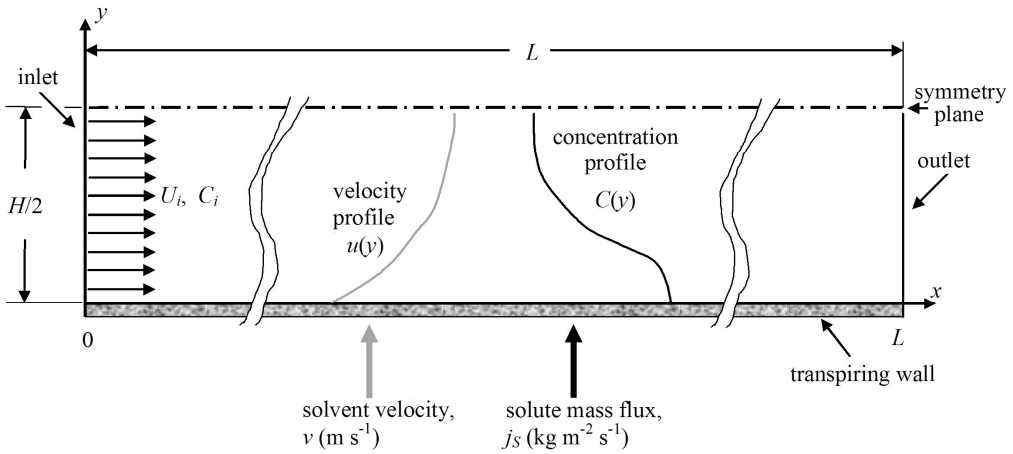

Figure 7. Computational domain (plane channel of length L and thickness H with transpiring walls). Generic velocity and concentration profiles are shown. Both solute and solvent fluxes are regarded as positive if they are directed into the channel. U_i, C_i are uniform inlet velocity and concentration.

A preliminary analysis of the problem shows that Sh depends on the following dimensionless numbers:

Reynolds number	$\mathrm{Re}=U_i d_{eq} \rho / \mu$
Schmidt number	$\mathrm{Sc}=\mu/(\rho D)$
Flux number	$\mathrm{Fl}=j_S/(\rho U_i C_i)$
Transpiration number	$\mathrm{Tr}=v/U_i$
Distance from inlet	x/d_{eq}

Further dimensionless numbers, e.g. the flow Péclet number Pe=Re·Pr and the transpiration Péclet number Pe_{tr}=Pe·Tr, can be derived from the above ones. The transpiration number Tr expresses the importance of the transpiration cross-flow with respect to the main axial flow, and is similar to the "blowing factor" used in the analysis of transpired boundary layers [1]. Note that it is positive for blowing (injection), negative for suction. Similarly, the flux number Fl expresses the importance of the solute mass flux crossing the walls with respect to the solute mass flux advected into the channel by the main flow; also Fl can be positive for mass flow into the channel, negative for mass flow out of it.

U_i and C_i in the above definitions are the *inlet* values of velocity and concentration. For small flow / transpiration numbers and moderate distances from the inlet, these values will not appreciably differ from the local ones U, C_b. Similarly, in general the physical properties ρ, μ, D are functions of concentration C and thus may vary both along the channel and across it; in this study, for the purpose of simplicity, they were assumed constant. Finally, note that either the mass flux j_S or the wall concentration C_w can be imposed as boundary conditions, while the other quantity will be a result of the exchange phenomena occurring in the channel.

The parameter x/d_{eq} is appropriate for *local* values of Sh, and can be replaced by the slenderness ratio L/d_{eq} if *average* values are required instead.

In its turn, Sh can be normalized to the value Sh_0 that would hold in the absence of transpiration (Tr=0), yielding $\mathrm{Sh}^*=\mathrm{Sh}/\mathrm{Sh}_0$. For parallel flow in plane channels of infinite span, Sh_0 is ~8.24 for uniform wall mass flux and ~7.54 for uniform wall concentration [12].

In an internal-flow configuration like that considered here, solvent and solute fluxes cannot be made to vary arbitrarily, but must obey some physical limitations. In particular, in the case of suction v (<0) is limited by the requirement that the solvent flow rate must remain positive at the outlet $x=L$,

which imposes $v \geq -(U_i/4)/(L/d_{eq})$ ("voiding" limit). Similarly, in the case of solute flux out of the channel, j_S (<0) is limited by the condition that the solute mass flow rate must remain positive at the outlet, which imposes $j_S \geq -(\rho U_i C_i/4)/(L/d_{eq})$ ("desalting" limit). In terms of the dimensionless numbers Tr, Fl, the above limitations translate into

$$\mathrm{Tr} \geq -\frac{1/4}{L/d_{eq}} \qquad \text{("voiding" limit)} \tag{7}$$

$$\mathrm{Fl} \geq -\frac{1/4}{L/d_{eq}} \qquad \text{("desalting" limit)} \tag{8}$$

For the channel under study, with $L/d_{eq}=1000$, the common lower limit of Tr and Fl is $-2.5 \cdot 10^{-4}$.

For positive transpiration (injection) and/or solute flux there are, in principle, no such limits. In real applications, further limits may arise by the requirement that the concentration does not exceed the solubility limit ($C \leq C_{sat}$). Note also that, if the cross-stream concentration profiles are taken into account, the physical requirement that the concentration remains positive everywhere across the channel will impose limits more stringent than those expressed by Eqs. (7)-(8).

3.2 Approximate solutions

In general, the presence of transpiration distorts the cross stream profiles of both axial velocity $u(y)$ and concentration $C(y)$ with respect to the non-transpiring case, making the analysis difficult and making at least a two-dimensional computational approach necessary.

A great simplification is obtained by assuming that concentration profiles across the channel are not significantly perturbed by transpiration, i.e. remain self-similar at different values of Tr. Figure 8 shows such C profiles, normalized as $(C-C_b)/(C_w-C_b)$, computed at $x/d_{eq}=500$ for Re=8, Sc=500 (Pe=4000), Fl/Tr=2 and increasing values of the transpiration number Tr, from 0 to 10^{-2}. These profiles were obtained by two-dimensional CFD simulations, as discussed in the next Section 3.3. For symmetry reasons, only one half of the channel ($0 \leq y/H \leq 0.5$) is shown. It can be observed that up to $\mathrm{Tr} \approx 10^{-3}$ concentration profiles remain basically self-similar, while at higher values of Tr they develop an inflection point and become flat in the proximity of the wall.

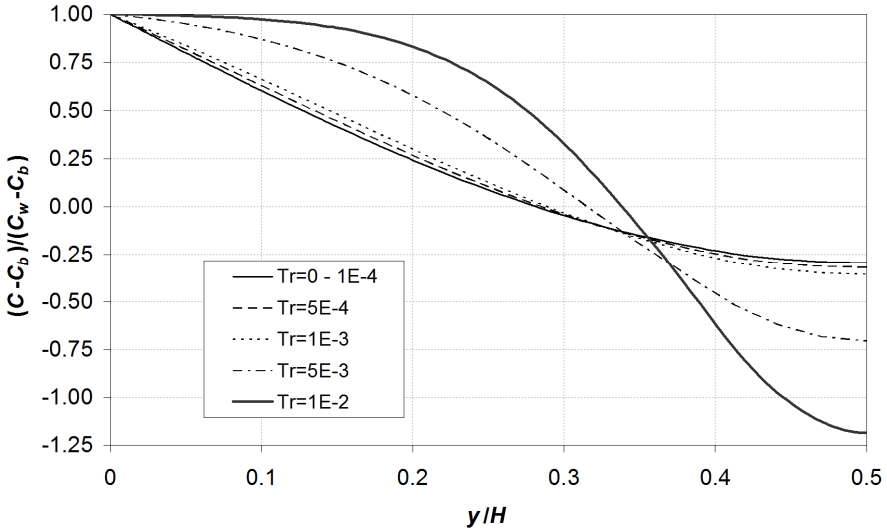

Figure 8. Cross stream profiles of concentration, normalized as $(C-C_b)/(C_w-C_b)$, computed by 2-D CFD for Sc=500, Re=8, $x/d_{eq}=500$, Fl/Tr=2 and increasing values of the transpiration number Tr from 0 to 0.01.

The results in Figure 8 were obtained for Sc=500. A more complete analysis, including different values of Sc and negative values of Tr, shows that the assumption of self-similar concentration profiles holds provided Sc·|Tr|«1. For example, for Sc=1 a significant departure from self-similarity would occur only at unlikely transpiration velocities of the same order as the inlet velocity. Similarly, normalized velocity profiles remain very close to Poiseuille profile provided |Tr|«1.

As long as normalized concentration profiles remain close to that holding in the absence of transpiration, also the diffusion Sherwood number Sh_{diff} defined by Eq. (3) remains close to the theoretical value Sh_0 for Tr=0 (e.g. ~8.24 for plane channels with uniform imposed wall mass flux). Figure 9 shows Sh_{diff} as a function of the transpiration number, computed by 2-D CFD under the same conditions as Figure 8 (x/d_{eq}=500, Re=8, Sc=500, Fl/Tr=2). It can be observed that Sh_{diff} remains approximately constant up to Tr≈10^{-4}, while, for Tr higher than ~10^{-3}, it falls rapidly and becomes negligible for Tr=10^{-2}.

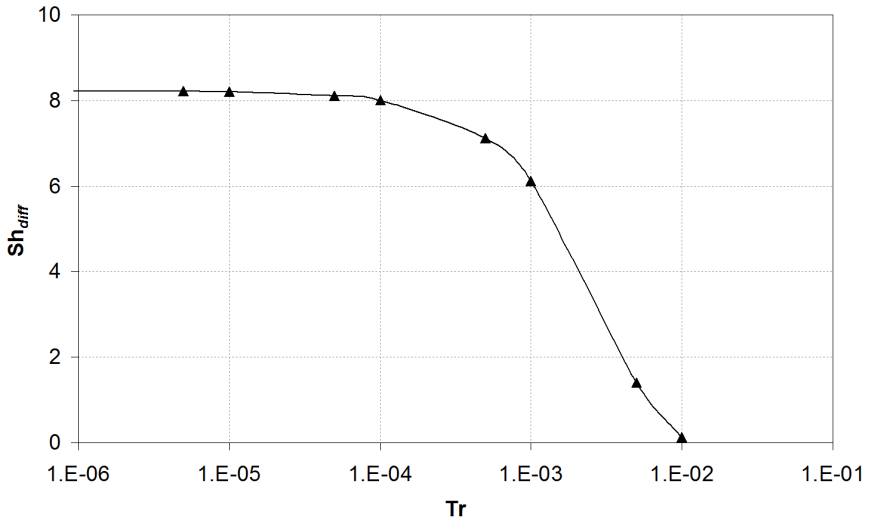

Figure 9. Diffusive Sherwood number Sh_{diff} as a function of the transpiration number Tr, computed by 2-D CFD for Sc=500, Re=8, x/d_{eq}=500, Fl/Tr=2.

Under the assumption of Sh_{diff}=Sh_0, one has j_{diff}=$Sh_0(C_w$-$C_b)\rho D/d_{eq}$. Adding the convective flux $\rho v C_w$ to obtain the total mass flux j_S and making it dimensionless as a Sherwood number, one has:

$$\mathrm{Sh} = \mathrm{Sh}_0 + \frac{C_w}{(C_w - C_b)} \cdot \mathrm{Tr} \cdot \mathrm{Pe} \tag{9}$$

Normalizing by Sh_0 and identifying C_b with C_i (see above remarks on this issue), with some manipulations the following expression is obtained:

$$\mathrm{Sh}^* \equiv \frac{\mathrm{Sh}}{\mathrm{Sh}_0} = \frac{1 + \mathrm{Tr} \cdot \mathrm{Pe} / \mathrm{Sh}_0}{1 - \mathrm{Tr} / \mathrm{Fl}} \tag{10}$$

Eq. (10) shows that, under the present assumption of self-similar concentration profiles, Sh^* is a function of the three dimensionless numbers Fl, Tr and Pe. For a given value of Pe, an isoline map of Sh^* can be plotted in the plane (Tr, Fl) as shown in Figure 10 for Pe=10^4. The surrounding insets schematically show the direction of solvent and solute fluxes and the concentration profile associated to each value (or range of values) of the polar coordinate θ.

The left and lower boundaries of the map correspond to the "voiding" and "desalting" limits expressed by Eqs. (7)-(8), while in the top and right directions the map is, in principle, unlimited.

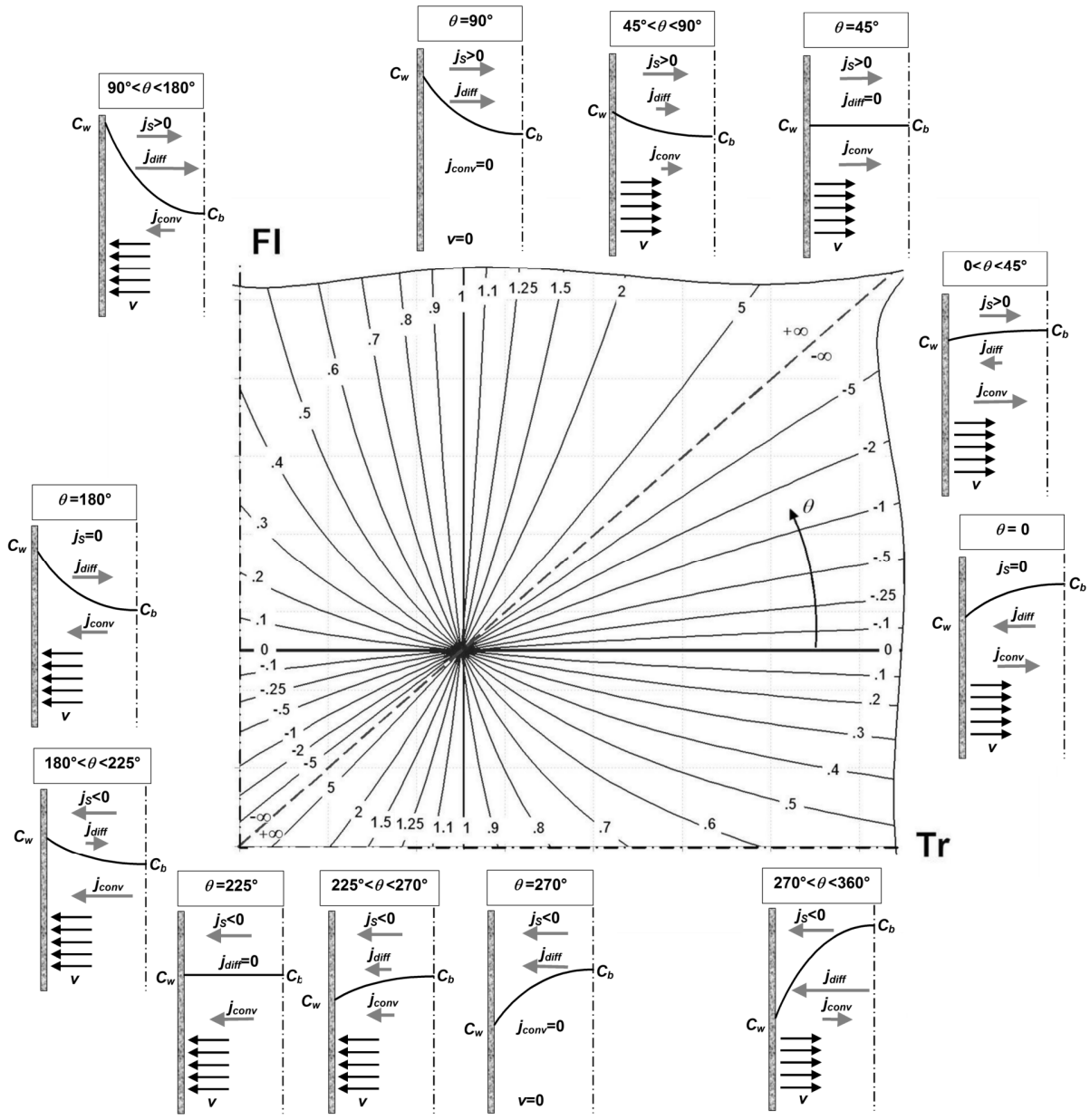

Figure 10. Lines Sh^*=constant in the (Tr, Fl) plane for $Pe=10^4$.

The map can be divided into several regions according to the sign of Tr and Fl and to the values attained by the normalized Sherwood number Sh^*.

- For $\theta=0$, i.e. along the horizontal axis Fl=0, the net solute flux is nil but a solvent transpiration flux exists (except at the origin), creating a concentration profile and a (negative) concentration drop $\Delta C=C_w-C_b$. Therefore, here one has Sh=0. The origin itself is obviously a singular case in which neither solvent nor solute fluxes exist and Sh is undefined.
- For $0<\theta<45°$, both the solute and the solvent fluxes are positive (Tr>0, Fl>0) but the convective solute flux is larger than the diffusive one (Tr>Fl) so that the wall concentration becomes lower than the bulk concentration, yielding $\Delta C<0$ and thus Sh<0.

- For θ=45°, i.e. along the bisecting line Fl=Tr (with Fl>0, Tr>0), the solute influx is purely covective, so that ΔC=0 and Sh diverges to -∞ on the side θ<45° and to +∞ on the side θ>45°.
- For 45°<θ<90°, both the solute and the solvent fluxes are still positive (Tr>0, Fl>0), but the convective solute flux is less than the diffusive one (Tr<Fl); the result is a reduction of ΔC and an increment of Sh with respect to the non-transpiring case (Sh>Sh_0). This is the range in which blowing promotes mass or heat transfer from the wall to the fluid.
- For θ=90°, i.e. along the vertical axis (Tr=0, Fl>0), the classic condition of mass transfer from the wall to the fluid without transpiration is recovered, and Sh attains its reference value Sh_0 (~8.24 in plane channels with uniform mass flux at the walls).
- For 90°<θ<180°, one has Tr<0, Fl>0; the convective solute flux is negative but less, in absolute value, than the diffusive solute flux; for a given total solute flux, the diffusive component and C_w-C_b are larger than for θ=90°, so that Sh becomes less than Sh_0. This is the range in which suction inhibits mass or heat transfer from the wall to the fluid.
- The case θ=180° (left part of the horizontal axis Fl=0) is similar to the case θ=0: the solute flux is nil but a negative solvent transpiration flux exists, creating a concentration profile and a (positive) concentration drop C_w-C_b. Therefore, Sh=0. This case is, basically, that discussed in Section 2.3 for reverse osmosis or filtration (Figure 6).
- For 180°<θ<225°, both the solute and the solvent fluxes are negative (Tr<0, Fl<0) but the convective solute flux dominates over the diffusive one ($|\mathrm{Tr}|>|\mathrm{Fl}|$), so that the wall concentration becomes higher than the bulk concentration, yielding Sh<0.
- For θ=225°, i.e. along the bisecting line Fl=Tr (with Fl<0, Tr<0), the solute flux is purely convective, so that C_w-C_b=0 and Sh diverges to -∞ on the side θ<225° and to +∞ on the side θ>225°.
- For 225°<θ<270°, both the solute and the solvent fluxes are still negative (Tr>0, Fl>0), but the solvent inflow is relatively small ($|\mathrm{Tr}|<|\mathrm{Fl}|$); the result is a reduction of $|C_w\text{-}C_b|$ (C_w-C_b is negative) and an increment of Sh with respect to the non-transpiring case (Sh>Sh_0). This is the range in which suction promotes mass or heat transfer from the fluid to the wall.
- For θ=270°, i.e. along the vertical axis (Tr=0, Fl<0), the classic condition of mass transfer from the fluid to the wall without transpiration is recovered, as in the case θ=90°, and Sh attains its reference value Sh_0.
- Finally, for 270°<θ<360°, one has Tr>0, Fl<0; the convective solute flux at the wall is positive but less, in absolute value, than the total (negative) solute flux; for a given total solute flux, the diffusive component and $|C_w\text{-}C_b|$ increase (C_w-C_b is negative), so that Sh becomes less than Sh_0. This is the range in which blowing inhibits mass or heat transfer from the fluid to the wall (e.g. transpiration cooling).

Note that the singularities at θ=45° and 225° correspond to the condition Fl=Tr. Under this condition, the combined effect of solvent and solute inflow or outflow is equivalent to the inflow or outflow of solution having a concentration equal to the bulk concentration in the channel, a condition for which j_S≠0 but C_w-C_b=0, whence Sh=±∞.

Figure 10 suggests that Sh^* is mainly a function of the polar coordinate θ. In fact, an analysis of Eq. (10) shows that, for small values of the group $\mathrm{Tr}\cdot\mathrm{Pe}/Sh_0$, one has $Sh^*=(1-\mathrm{Tr}/\mathrm{Fl})^{-1}$, i.e. Sh^* is a function of the single dimensionless number Fl/Tr (ratio of flow and transpiration numbers), which is obviously related to θ by $\mathrm{Fl}/\mathrm{Tr}=\tan(\theta)$. For larger values of $\mathrm{Tr}\cdot\mathrm{Pe}/Sh_0$, Sh^* in Eq. (10) becomes a function of Tr and Fl separately, and not only of their ratio. This behaviour corresponds to the departure of the iso-lines in Figure 10 from straight lines crossing the origin, a departure which is particularly visible in the second and fourth quadrants where Fl and Tr have opposite signs.

Figure 11 reports the normalized Sherwood number along a circle of radius 10^{-4} in the (Tr, Fl) plane for Pe ranging from $3\cdot10^3$ to 10^5. It can be observed that, for Pe up to ~10^4-$3\cdot10^4$, Sh^* does not appreciably depend on the Péclet number. Also, for such small values of Pe, the function $Sh^*(\theta)$ is periodic with period 180°, so that the simultaneous reversal of Tr and Fl leaves Sh unchanged. At higher Pe (e.g. 10^5) Sh* becomes a function of Pe and the 180°-periodicity is lost.

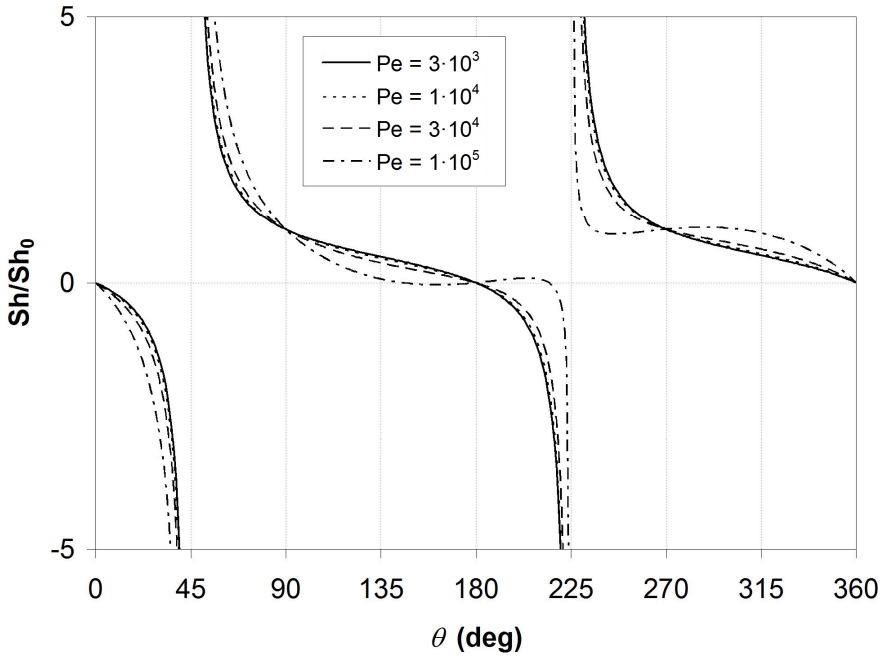

Figure 11. Normalized Sherwood number as a function of the azimuthal angle θ (see Figure 10) for $(Tr^2+Fl^2)=10^{-8}$ and different values of the Péclet number, ranging from $3\cdot10^3$ to 10^5.

3.3 CFD approach

If the assumption of self-similar concentration profiles cannot be made, i.e., if the product Sc·Tr exceeds ~0.5, more general methods must be adopted. In general, fluid flow and solute transport in the channel are governed by the continuity, momentum (Navier-Stokes) and solute transport equations, which can be written, in steady-state form and neglecting body forces and solute source terms, as:

$$\frac{\partial \rho u_j}{\partial x_j} = 0 \tag{11}$$

$$\frac{\partial \rho u_i u_j}{\partial x_j} = -\frac{\partial p}{\partial x_i} + \frac{\partial}{\partial x_j}\mu\left(\frac{\partial u_i}{\partial x_j} + \frac{\partial u_j}{\partial x_i}\right) \tag{12}$$

$$\frac{\partial \rho u_j C}{\partial x_j} = \frac{\partial}{\partial x_j}\rho D\frac{\partial C}{\partial x_j} \tag{13}$$

Here, C is the solute mass fraction; the solvent mass fraction is, of course, 1-C. Two different approaches are possible.

a) C can be regarded as the concentration of a *massless passive scalar* and Dirichlet, Neumann or mixed (Robin) conditions for C are applied at the walls to simulate solute transfer, while a Dirichlet condition of nonzero normal velocity is imposed to **u** in order to to simulate transpiration (the parallel component of **u** is assumed to be zero at walls for the no slip condition). By this approach, the contribution of the solute to mass balance is neglected, which is clearly wrong if the solute mass flux, integrated over the walls, is a significant fraction of the total mass flow rate.

b) The solution can be treated as a *variable composition mixture* made up of two components: solute, with mass fraction C, and solvent, with mass fraction 1-C. The two components share a common velocity field **u**, as in homogeneous two-phase flow, so that the momentum equations (30) remain valid. The continuity equation (11) is replaced by separate continuity equations for the two

components. Solute transport is still governed by Eq. (13), including diffusion terms. The flux of each component through the walls is described by suitable boundary mass sources expressing the mass flow rate of that component (positive if directed from wall to fluid, negative if directed from fluid to wall). This treatment allows the contribution of solute to mass balance correctly to be taken into account.

Both models were implemented into the finite volume Ansys-CFX® CFD code. The two methods yielded similar results for small inlet-outlet solute mass flow rate variations, but differ significantly otherwise. The variable composition mixture approach was preferred for its greater generality. Note that neither model distinguishes between a "true" solution (i.e., a dispersion at molecular level, as may occur with salt water) or a heterogeneous, two-phase, dispersion (as may occur with suspended particles), provided the scale of the dispersion is sufficiently small for inter-phase slip to vanish and a single flow field to apply to both components. Therefore, for example, filtration problems at various scales can be treated in the same framework as electrodialysis or reverse osmosis.

In either approach, the solution physical properties (density ρ, viscosity μ) and the solute diffusivity D – or, equivalently, the Schmidt number $(\mu/\rho)/D$ – should be expressed as functions of the concentration C, especially in the presence of strong spatial variations of this quantity. For example, for fresh water at 25°C one has ρ=997 kg m^{-3}, μ=0.890·10^{-3} Pa·s, while for seawater (salt mass fraction ~0.03) one has ρ=1017 kg m^{-3}, μ=0.931·10^{-3} Pa·s. However, as mentioned above, in the present study we assumed constant values of the properties (in most cases ρ=1000 kg m^{-3}, μ=0.9·10^{-3} Pa·s, Sc=500), mainly in order to avoid unnecessary complications in interpreting the results.

Symmetry conditions were imposed at the centreline. Dirichlet conditions $u=U_i$, $C=C_i$ were imposed at the inlet for axial velocity and concentration. At the outlet, a uniform pressure p_0 was imposed for the flow field and fully developed Neumann conditions ($\partial/\partial x$=0) for the concentration field C. As discussed above, at the transpiring wall solute and solvent fluxes were represented as boundary mass sources for the two components. The concentration profiles in Figure 8 and the behaviour of Sh_{diff} with Tr in Figure 9, used to assess the limits of applicability of the approximate method of Section 3.2, are examples of the results provided by CFD.

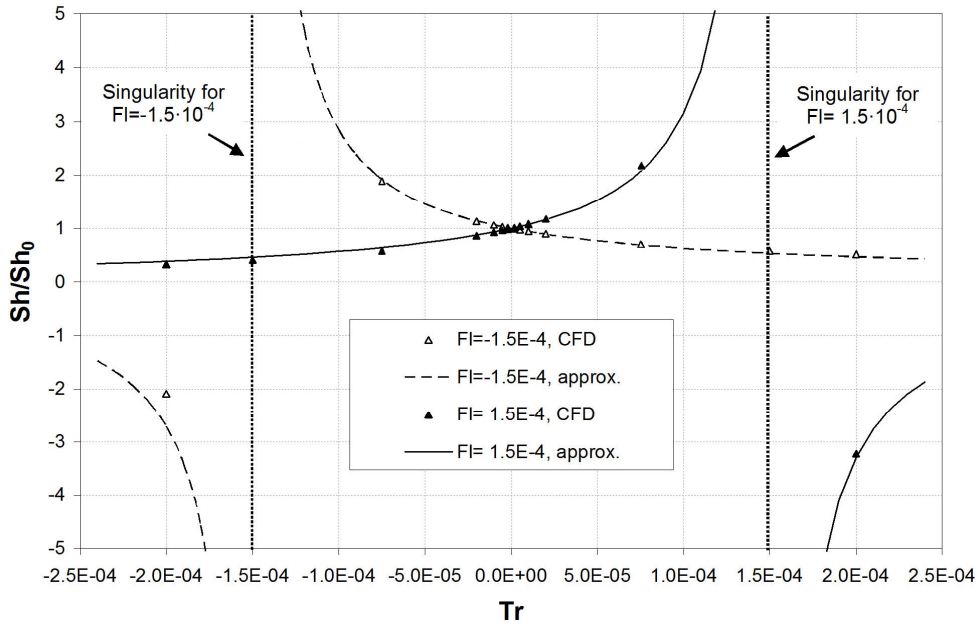

Figure 12. Sherwood number as a function of the transpiration number for flux numbers Fl=±1.5·10^{-4}. Approximate predictions provided by Eq. (10) are compared with CFD results. Hollow symbols and dashed line: Fl=-1.5·10^{-4}; solid symbols and solid line: Fl=1.5·10^{-4}.

A comparison of CFD results and approximate predictions provided by Eq. (10) (obtained under the assumption of self-similar concentration profiles, i.e. diffusion Sherwood number unaffected by transpiration) is shown in Figure 12. For flux numbers Fl of $-1.5\cdot10^{-4}$ (solute out of the channel) and $1.5\cdot10^{-4}$ (solute into the channel), the normalized Sherwood number $Sh^{*}=Sh/Sh_0$ is reported as a function of the transpiration number Tr in the range from $-2\cdot10^{-4}$ to $2\cdot10^{-4}$.

Figure 12 shows that the predictions of the approximate model agree well with CFD results in the range considered, which for Sc=500 complies with the above mentioned criterion $Sc\cdot|Tr|\ll1$. Predictions (either by the approximate model or by CFD) should be taken with some caution in the proximity of the singularities Tr=Fl.

As a further example of the results obtained by the 2-D CFD approach, Figure 13 reports axial profiles of the Sherwood number along the channel walls for flux numbers $Fl=-1.5\cdot10^{-4}$ (a) or $Fl=1.5\cdot10^{-4}$ (b) and transpiration numbers increasing from $-2\cdot10^{-4}$ to $2\cdot10^{-4}$. The abscissa is the normalized axial coordinate x/L.

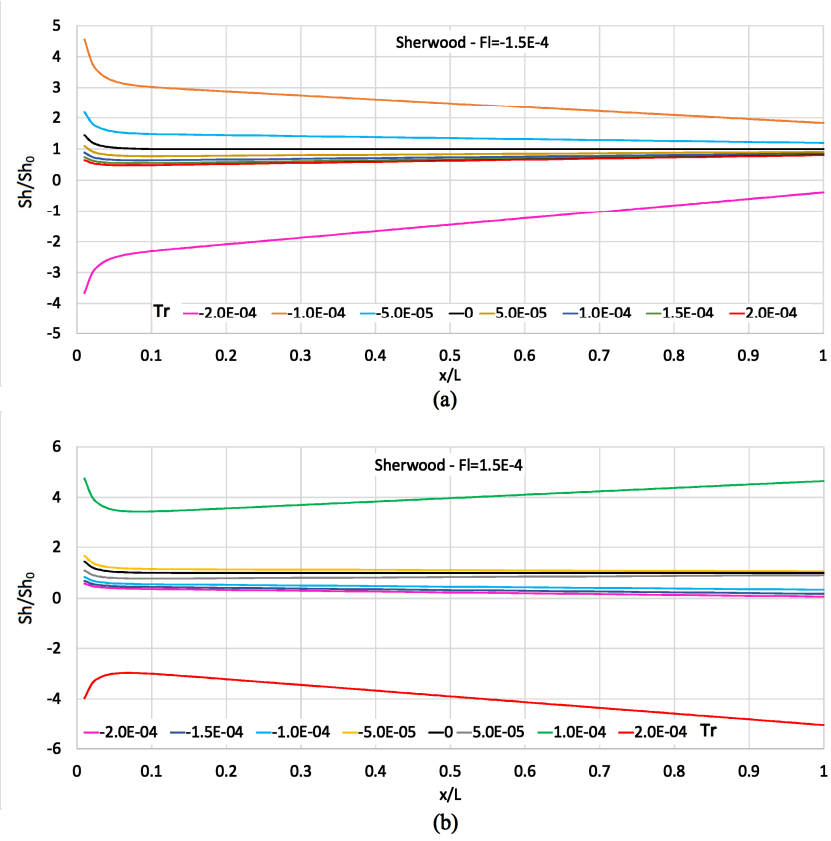

Figure 13. CFD results: axial profiles of the Sherwood number (normalized to Sh_0) along the channel walls for flux numbers $Fl=-1.5\cdot10^{-4}$ (a) or $Fl=1.5\cdot10^{-4}$ (b) and transpiration numbers ranging from $-2\cdot10^{-4}$ to $2\cdot10^{-4}$.

In Figure 13, the sign of Sh for each combination of Fl and Tr can easily be interpreted in the light of Figures 10 and 11. A noteworthy feature of the results is that, in the presence of transpiration, the Sherwood number does not attain a constant value after entry effects are extinguished (see below), but continues to vary (almost linearly) along the channel. More precisely, as x increases, the Sherwood number profiles obtained for different Tr tend to converge to Sh_0 when the flux number Fl is negative (solute flux out of the channel), whereas they diverge when Fl is positive (solute entering the channel). The reason for this behaviour is that, while the total solute flux is imposed to be uniform along the channel, the two separate diffusive and convective components vary, and so does the wall-bulk concentration difference.

Entrance effects proper extend over a limited portion of the channel length, in accordance with the Graetz theory [13]. For non-transpired channel flow, this predicts that the local Sherwood number decreases towards its fully developed value Sh_∞ as a function of the dimensionless distance from inlet, $x^*=(x/d_{eq})/Pe$. The Sh/Sh_∞ ratio becomes negligibly different from unity (e.g., ≤1.05) for $x^*>0.02$. In the present configuration, due to the high value of Sc (500) and despite the low values of Re (e.g. 8), Pe is relatively high (e.g. 4000), so that the condition $x^*=0.02$ is attained for $(x/d_{eq})=80$. For H=300 μm (d_{eq}=600 μm) and L=0.6 m, this value corresponds to a distance of 0.048 m, or 0.08 L, from inlet. The results in Figure 13 agree well with these estimates for all values of Tr, confirming that the Graetz theory basically holds also in the presence of transpiration.

4. Conclusions

The general problem of mass transfer between a fluid stream and a wall in the presence of cross-stream flow (wall transpiration) was examined. In the introductory sections of this paper, a suitable notation was introduced, based on separately considering the fluxes of two components, a "solvent" and a "solute", through the wall. Possible configurations were classified according to the combined signs of the two fluxes, and special or singular conditions (of which simple mass transfer with no transpiration is just an example) were identified. Examples from engineering, notably from membrane-based processes, were given for several of the more complex flux combinations; they include, among others, direct and reverse electrodialysis, reverse osmosis and filtration. The analogy with heat transfer processes involving transpiration (e.g. transpiration cooling) was also briefly discussed.

In the bulk of the paper, the attention was focussed on a specific configuration, namely, two-dimensional Poiseuille flow in a slender channel with simultaneous solute flux and solvent transpiration at the walls. Besides the common dimensionless parameters occurring in no-transpiration problems, such as the Reynolds, Schmidt, Péclet and Sherwood numbers Re, Sc, Pe, Sh and the channel slenderness ratio L/d_{eq}, new dimensionless numbers appropriate to transpiration problems were introduced. These include a transpiration number (Tr) and a flow number (Fl), respectively expressing the importance of the transpiration solvent flux and of the total solute flux through the walls with respect to the inlet flow rate and advective solute flux. For negative Tr and Fl, limiting values of these numbers, associated to what can be called the "voiding" and "desalting" conditions, were identified as functions of the channel slenderness.

The subsequent analysis was conducted for a high Schmidt number (500) and proceeded along two parallel directions.

On one side, the problem was analysed by two-dimensional computational fluid dynamics using a finite volume method. Solute transport was modelled by two different approaches: the former treated the solute as a passive and massless scalar, while the latter treated the solution as a variable composition mixture with separate continuity equations for solvent and solute. The two treatments converged for low concentrations, but only the latter properly accounted for the contribution of the solute to the solution mass balance (important at high concentrations), and thus was preferred in the generality of the cases.

On the other side, a simplifying assumption was adopted, namely, that the transpiration flow does not significantly affect concentration profiles and thus diffusive Sherwood numbers. By comparison with CFD simulations, this assumption was found to hold to an acceptable degree as far as the product of the Schmidt number and the transpiration number, $Sc \cdot Tr$, is (in absolute value) much smaller than unity. By adopting this approximation, simple algebraic manipulations led to an expression relating the Sherwood number to the transpiration, flux and Péclet numbers (Eq. 10). The comparison of the approximate theory with CFD results (in which no such approximation was used) showed a good agreement provided the condition $Sc \cdot |Tr| \ll 1$ was met.

By using the approximate theory, a complete map was drawn of the Sherwood number in the (Fl, Tr) plane for a given value of Pe. Different regions were identified, and the directions of the diffusive, convective and total solute flux (along with the shape of concentration profiles) associated with each region were highlighted. *Loci* of singularity, associated with Sh diverging to $\pm\infty$, occurred in correspondence with the line Fl=Tr, where the combined flux of solute and solvent through the walls

is equivalent to the inflow or outflow of solution at the same concentration as that flowing in the channel.

Finally, using CFD results, profiles of the Sherwood number along the streamwise direction were obtained for different values of the flux and transpiration numbers. A noteworthy feature of these curves was that, unlike in non-transpired channel flow, Sh did not settle to a fully developed value but continued to evolve along the channel as a consequence of the axial variation of the flow rate.

NOMENCLATURE

Symbol	Quantity	Unit
C	Concentration	kg kg^{-1}
C_f	Fanning friction coefficient	-
D	Solute diffusivity	m^2 s^{-1}
d_{eq}	Hydraulic diameter (=2H)	m
Fl	Flux number, $j_S/(\rho U C_b)$	-
H	Channel thickness	m
j	Mass flux	kg m^{-2} s^{-1}
k	Mass transfer coefficient	m s^{-1}
L	Channel length	m
p	Pressure	Pa
Pe	Péclet number, Re·Pr or Re·Sc	-
Re	Reynolds number, $U\, d_{eq}\rho/\mu$	-
Sc	Schmidt number, $\mu/(\rho D)$	-
Sh	Sherwood number, $k \cdot d_{eq}/D$	-
St	Stanton number, Nu/(Re·Pr) or Sh/(Re·Sc)	-
Tr	Transpiration number, v/U	-
U	Cross-section-averaged velocity	m s^{-1}
U_∞	Free stream velocity	m s^{-1}
u_j	Generic velocity component	m s^{-1}
u	Velocity vector	m s^{-1}
v	Transpiration velocity	m s^{-1}
x	Distance from inlet or leading edge	m
y	Co-ordinate orthogonal to the wall	m

Greek symbols

Δp	Pressure difference	Pa
$\Delta\pi$	Osmotic pressure difference	Pa
θ	Azimuthal coordinate in (Tr, Fl) plane	deg
μ	Solution viscosity	Pa s
π	Osmotic pressure	Pa
ρ	Solution density	kg m^{-3}
σ	Rejection coefficient	-

Subscripts/superscripts

b	Bulk

conv	convective
diff	Diffusive
i	Inlet
S	Solute
tr	Transpiration
W	Water
w	Wall
0	No transpiration value
*	Normalized to the no transpiration value

References

[1] W. M. Kays, R. J. Moffat, *The behaviour of transpired turbulent boundary layers*, Report No. HMT-20, Thermosciences Division, Department of Mechanical Engineering, Stanford University, Stanford, CA, April 1975.

[2] R. N. Meroney, *Laminar/turbulent transition in transpired boundary layers*, Final report, NSF Grant ENG-70-01360 (GK 23989), Fluid Dynamics and Diffusion Laboratory, College of Engineering, Colorado State University, Fort Collins, CO, December 1974.

[3] J. Polezhaev, The transpiration cooling for blades of high temperatures gas turbine, *Energy Convers. Mgmt* **38** (1997), 1123-1133.

[4] R. W. Newman, R. W. Allen, Compact transpiration cooling systems, *APL Technical Digest* (may-june 1972) 13-21.

[5] P. A. Marrone, M. Hodes, K. A. Smith, J. W. Tester, Salt precipitation and scale control in supercritical water oxidation—part B: commercial/full-scale applications, *J. of Supercritical Fluids* **29** (2004) 289–312.

[6] J. C. de la Rosa, L. E. Herranz, J. L. Muñoz-Cobo, Analysis of the suction effect on the mass transfer when using the heat and mass transfer analogy, *Nucl. Eng. and Design* **239** (2009) 2042–2055.

[7] T.-F. Zien, *Approximate analysis of heat transfer in transpired boundary layers at limiting Prandtl numbers*, Report No. AD-785 239, Naval Ordnance Laboratory, White Oak, MD, 1 July 1974.

[8] M. F. La Cerva, M. Di Liberto, L. Gurreri, A. Tamburini, A. Cipollina, G. Micale, M. Ciofalo, Coupling CFD with simplified 1-D models to predict the performance of Reverse Electrodialysis stacks, *Journal of Membrane Science* **541** (2017) 596-610.

[9] A. Campione, L. Gurreri, M. Ciofalo, G. Micale, A. Tamburini, A. Cipollina, Electrodialysis for water desalination: a critical assessment of recent developments on process fundamentals, models and applications, *Desalination* **434** (2018) 121-160.

[10] S. S. Sablani, M. F. A. Goosen, R. Al-Belushi, M Wilf, Concentration polarization in ultrafiltration and reverse osmosis: a critical review, *Desalination* **141** (2001) 269-289.

[11] M. Amokrane, D. Sadaoui, C. P. Koutsou, A. J. Karabelas, M. Dudeck, A study of flow field and concentration polarization evolution in membrane channels witht wo-dimensional spacers during water desalination, *Journal of Membrane Science* **477** (2015) 139–150.

[12] M. Ciofalo, M. F. La Cerva, M. Di Liberto, A. Tamburini, Influence of the boundary conditions on heat or mass transfer in complex channels, *J. of Physics Conf. Ser.* **923** (2017), 012053.

[13] V. Gnielinski, *VDI-Wärmeatlas*, Springer-Verlag, Berlin, 1997.